Reliability Analysis of Vertical Joints of Steel Plate-Concrete Composite Silo Wall in Assembled Underground Granary

Hao Zhang[1,a], Xu Gao[1,b], Lei Chen[1,c]

[1] College of Civil Engineering, Henan University of Technology, Zhengzhou 450001, China
[a]zhanghaotm@haut.edu.cn;
[b]18839417089@163.com;cchenlei@haut.edu.cn

Abstract. The structural configuration and mechanical characteristics of steel plate-concrete composite wall joints pose significant challenges that hinder their widespread utilization. To investigate the reliability of vertical joints in prefabricated underground grain silos featuring trapezoidal force-transmitting steel plates within steel plate-concrete composite walls, a structural reliability analysis was conducted utilizing extensive finite element simulation data. This analysis entailed reducing the concrete strength, steel plate strength, and IWST(thickness of inner waterproof steel plate), thereby simulating structural deficiencies in the test specimens. The results show that the parameters that affect the reduction coefficient of the bearing capacity of the specimen from large to small are concrete strength, steel plate strength and IWST. It is suggested that in practical engineering, the design strength of the concrete of the silo wall joint should be C50, the steel plate strength should be Q345, and the IWST should be 10 mm.

Keywords: Reliability; bending performance; finite element; parametric analysis; joint

1 Introduction

Compared with the traditional aboveground granary, underground grain storage has significant advantages such as high safety, resource saving and environmental friendly [1]. At present, many scholars have achieved fruitful results in the research field of underground granaries, but underground granaries still face a series of problems, such as high standards of waterproof and moistureproof requirements, long construction period caused by wet working environment of deep foundation pit, and high cost of foundation pit support. In order to solve the above problems , Wang Zhenqing [2] and others proposed a large-diameter circular assembled steel plate-concrete composite structure scheme constructed by reverse construction method. This scheme solves the problems of waterproof and moistureproof of underground granary, deep foundation pit support, structural anti-floating and so on. Based on this scheme, a ' horn-shaped ' joint is proposed. However, this joint has too many steel plate welds, which is difficult to construct, and the amount of steel used is large and the cost is high, so it is difficult to apply

A. S. B. A Rashid et al. (eds.), *Proceedings of the 2024 3rd International Conference on Applied Mechanics and Engineering Structures (AMES 2024)*, Advances in Engineering Research 34,
https://doi.org/10.2991/978-94-6463-473-0_15

in actual construction. At present, there are few studies on the connection of the joint of the assembled underground granary wall. Some scholars have carried out a lot of research on the joints of similar assembled underground structures such as underground comprehensive pipe gallery [3,4], subway station [5,6], shield tunnel [7-9]. However, due to its different structural form and stress characteristics from the underground granary, it can only play a certain reference role.

Based on the research of the research group, this paper studies the joint form of the trapezoidal force transmission steel plate connection. The joint not only demonstrates excellent stress resistance and waterproofing capabilities, but it also significantly reduces the number of welds required, thereby saving on construction costs. In this paper, a finite element simulation using four-point bending loading is conducted on full-scale specimens of steel plate-concrete composite silo walls. Furthermore, a numerical analysis is performed to examine the parameters that influence the bearing capacity of these silo walls. On this basis, the bearing capacity and its corresponding deflection are used as the reliability index to analyze the structural reliability of the assembled underground granary joints.

2 Finite Element Module Method

2.1 Material Constitutive

The plastic damage model of concrete proposed (CDP model) by Lubliner [10] and Lee [11] is used in the constitutive model of concrete. In this model, the tensile damage and compressive damage of concrete adopt different damage factors to describe the stiffness degradation. It is assumed that the crack will close and the stiffness will recover when the concrete is stretched to compression, otherwise, the stiffness will not recover. The elastic modulus of concrete in the model is calculated by Formula 1.

$$\frac{10^5}{2.2+34.7/f_{cu}} \tag{1}$$

Where f_{cu} is cubic compressive strength of concrete.

The constitutive parameters obtained according to the CDP model are shown in Table 1.

Table 1. Constitutive parameters of concrete

poisson ratio	Expansion angle	Eccentricity	f_{b0}/f_{c0}	K	Viscosity parameter
0.2	38	0.1	1.16	0.667	0.002

The constitutive model of the steel plate is an ideal elastic-plastic model [12], which ignores the strain hardening phenomenon that may occur in the plastic stage of the steel, but the accuracy is within the allowable range of engineering calculation, which can accurately simulate the mechanical behavior of the steel under external force. adopted

by the steel plate ignores the strain hardening phenomenon that may occur in the plastic stage of the steel, but the accuracy is within the allowable range of engineering calculation, which can accurately simulate the mechanical behavior of the steel under external force. In this model, the elastic modulus of steel plate is 2.1×10^5MPa, the Poisson 's ratio is 0.3, and the yield strength is 420Mpa.

2.2 Unit selection and Grid Division

The C3D8R linear reduced integral element has been chosen for use in the stud, concrete, and steel plate simulations. In contrast to the complete integral element, the C3D8R variant features a single integral point positioned at the center of the element. This design significantly mitigates the risk of shear self-locking under bending loads, leading to more precise displacement solutions. Furthermore, even in the presence of grid distortion, the accuracy of the analysis remains largely unaffected. To address the potential expansion of the hourglass mode, a small amount of artificial hourglass stiffness is introduced, effectively limiting its impact.

The hexahedral element is used for structured meshing. The size of concrete, lining steel plate, U-shaped steel plate and inner and outer waterproof steel plate is 0.05 m, the size of force-transmitting steel plate is 0.02 m, and the size of Φ13 and Φ19 studs is 0.01 m, as shown in Fig. 1.

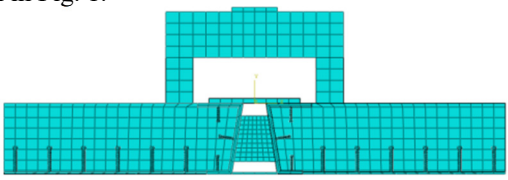

Fig. 1. Mesh generation of finite element model

2.3 Loading and Boundary Conditions

The specimen was subjected to four-point bending loading by simulating the distribution beam. By applying 30 mm displacement to each of the three points above the specimen, the direction of this displacement is oriented towards the negative direction of the Y-axis.

To ensure stability and prevent any unwanted movement or rotation during the loading process, the model is designed as a simply supported beam. Specifically, the displacements in the X, Y, and Z directions are constrained on the left side of the model, while only the displacements in the Y and Z directions are limited on the right side. The resulting finite element model is illustrated in Fig.2.

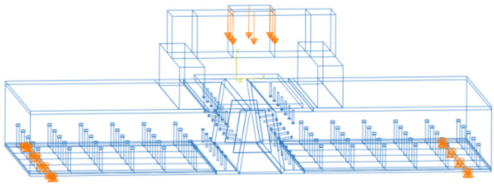

Fig. 2. Schematic diagram of finite element model

3 Reliability Analysis

From the previous research of the research group, it has been observed that the strength of concrete, the strength of steel plate and the thickness of inner waterproof steel plate are sensitive to the bearing capacity of the specimen[13]. The finite element model developed in the previous paper was used as the original model, and three different parameters were varied to simulate the damage occurring in the specimen, and the reliability of the specimen was analyzed by developing 27 finite element models.

Table 2. Design parameter values and main results

Serial number	Concrete strength /Mpa	Plate strength /Mpa	IWST /mm	Index of bearing capacity		Bearing capacity reduction coefficient	
				Peak load /kN	Deflection /mm	Finite element peak load/R_F	Deflection/R_D
0	60	420	14	2856.08	5.44738	1.0000	1.0000
1	30	390	12	2304.46	5.65872	0.8069	1.0388
2	30	390	10	2288.11	5.55647	0.8011	1.0200
3	30	390	8	2281.06	5.61887	0.7987	1.0315
4	30	345	12	2293.01	5.52192	0.8029	1.0137
5	30	345	10	2288.9	5.54147	0.8014	1.0173
6	30	345	8	2281.06	5.51521	0.7987	1.0125
7	30	235	12	2250.98	5.39509	0.7881	0.9904
8	30	235	10	2249.41	5.34978	0.7876	0.9821
9	30	235	8	2229.9	5.63349	0.7808	1.0342
10	40	390	12	2603.87	5.77631	0.9117	1.0604
11	40	390	10	2549.34	5.58835	0.8926	1.0259
12	40	390	8	2531.85	5.75966	0.8865	1.0573
13	40	345	12	2603.87	5.77631	0.9117	1.0604
14	40	345	10	2549.34	5.58835	0.8926	1.0259
15	40	345	8	2531.85	5.75966	0.8865	1.0573
16	40	235	12	2388.17	5.6314	0.8362	1.0338
17	40	235	10	2373.19	5.18422	0.8309	0.9517
18	40	235	8	2343.91	5.90347	0.8207	1.0837
19	50	390	12	2664.64	5.3752	0.9330	0.9867
20	50	390	10	2712.09	5.64991	0.9496	1.0372

21	50	390	8	2625.34	5.38311	0.9192	0.9882
22	50	345	12	2664.64	5.46411	0.9330	1.0031
23	50	345	10	2712.09	5.74328	0.9496	1.0543
24	50	345	8	2625.28	5.30286	0.9192	0.9735
25	50	235	12	2422.53	4.96058	0.8482	0.9106
26	50	235	10	2431.7	5.04148	0.8514	0.9255
27	50	235	8	2379.49	5.57976	0.8331	1.0243

Note: IWST is the abbreviation of the thickness of inner waterproof steel plate.

The reliability index of the specimen is defined from two aspects: the bearing capacity and the deflection corresponding to the bearing capacity (hereinafter referred to as deflection). The reduction factor R_F of the bearing capacity of the specimen is calculated as shown in formula 2.

$$R_F = \frac{M_0}{M} \tag{2}$$

Where M is the bearing capacity of the normal joint specimen, M_0 is the bearing capacity of the specimen with defects.

The calculation of the deflection reduction factor R_D of the specimen is shown in Formula 3.

$$R_D = \frac{T_0}{T} \tag{3}$$

Where T is the deflection of the normal joint specimen, and T_0 is the deflection of the specimen with defects.

According to Formula 2 and Formula 3, combined with the results of finite element simulation, the bearing capacity reduction coefficient and deflection reduction coefficient of each specimen are calculated, as shown in Table 2.

3.1 Influence of Concrete Strength on Reduction Factor of Bearing Capacity

Effect on Peak Load Reduction Factor

As shown in Fig.3, when the steel plate strength is Q390 and Q345, the influence of concrete strength on peak load is almost the same. When the strength of concrete is C30, the reduction coefficient changes greatly, indicating that the strength of structural concrete should be greater than C30. However, when the steel plate strength is Q235, the reduction factors of the three kinds of concrete strength are not much different, but the trend of the higher the concrete strength, the greater the reduction factor is still maintained. Given the strength of the chosen steel plate, it is observed that the specimen exhibits higher bearing capacity when the concrete strength reaches C50 and the IWST is 10 mm.

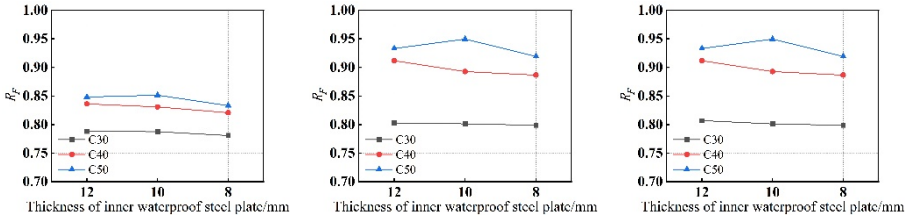

（a）Steel plate strength Q235　（b）Steel plate strength Q345　（c）Steel plate strength Q390

Fig. 3. Effect of concrete strength on R_F

Effect on the Deflection Reduction Factor

The greater the reduction coefficient of deflection, the smaller the bearing capacity, and the greater the bearing capacity. As shown in Fig.4, when the steel plate strength is Q390 and Q345, the influence of concrete strength on the deflection reduction coefficient is roughly the same. When the IWST is 10 mm, the deflection reduction coefficient decreases, but then increases. On the contrary, when the concrete strength is C50, the deflection reduction factor increases when the IWST is 10 mm, but it is generally smaller than the other two concrete strengths; when the steel plate strength is Q235, the deflection reduction coefficient of C50 concrete is the smallest under the same IWST. When the concrete strength is C40 and the IWST is 8mm, the deflection reduction coefficient is the largest.

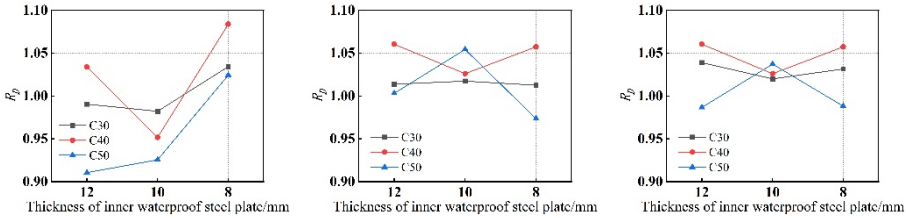

（a）Steel plate strength Q235　（b）Steel plate strength Q345　（c）Steel plate strength Q390

Fig. 4. Effect of concrete strength on R_D

Combined with the analysis, considering the load reduction coefficient and the deflection reduction coefficient, it is found that the bearing capacity reduction coefficient increases as the concrete strength increases, but the deflection reduction coefficient does not increase or decrease significantly, but when the concrete strength is the largest, the deflection reduction coefficient is relatively small.

3.2 The influence of steel plate strength on the reduction factor of bearing capacity

Effect on Peak Load Reduction Factor

As shown in Fig.5, when the steel plate strength is Q345 and Q690, the law of peak load reduction coefficient with the increase of concrete strength is almost the same, which basically satisfies the law that the greater the steel plate strength and concrete, the greater the reduction coefficient of bearing capacity under the same IWST. When the steel plate strength is greater than Q345, the strength of concrete and the IWST have little effect on the peak load reduction coefficient.

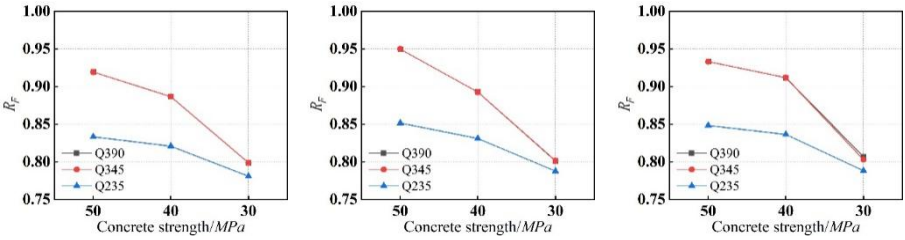

（a）The IWST is 8mm （b）The IWST is 10mm （c）The IWST is 12mm

Fig. 5. Effect of steel plate strength on R_F

Effect on the Deflection Reduction Factor

As shown in Fig.6, when the IWST is greater than 10 mm, the greater the strength of the steel plate, the smaller the deflection reduction coefficient of the structure, which indicates that the smaller the deflection of the structure, the safer the structure, but when the IWST is 8 mm, the greater the strength of the steel plate, the greater the deflection reduction coefficient, and when the concrete strength is C40, it has a poor cross-section bending stiffness. With the increase of the IWST and the strength of the steel plate, the deflection reduction coefficient of the specimen with the strength of Q345 steel plate changes little. Its structure is relatively stable.

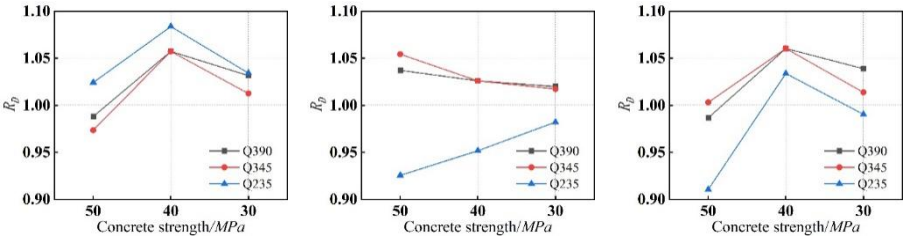

（a）The IWST is 8mm （b）The IWST is 10mm （c）The IWST is 12mm

Fig. 6. Effect of steel plate strength on R_D

In summary, increasing the steel plate strength has a great influence on the reduction coefficient of bearing capacity of specimens. The peak load reduction coefficient is

positively correlated with the strength of steel plate. When the steel plate strength is not less than Q345, the deflection reduction coefficient changes little with the strength of concrete and IWST. When the steel plate strength is Q235, the deflection reduction coefficient increases greatly. This is because when the steel plate strength decreases, its toughness is better, resulting in greater deflection and better ductility after reaching bearing capacity.

3.3 The Influence of the IWST on the Reduction Coefficient of Bearing Capacity

Effect on Peak Load Reduction Factor

As shown in Fig.7, with the increase of concrete strength, the influence of the IWST and the steel plate strength on the peak load reduction coefficient of the specimen gradually increases. And the greater the IWST, the smaller the impact.

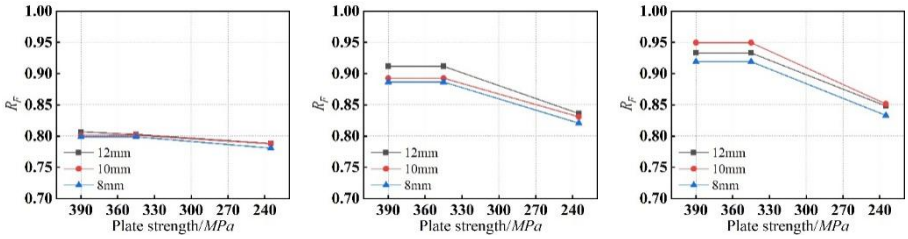

（a）The concrete strength is C30　（b）The concrete strength is C40　（c）The concrete strength is C50

Fig. 7. The influence of the IWST on R_F

Effect on the Deflection Reduction Factor

As shown in Fig.8, as a whole, when the IWST is 10 mm, changing the concrete strength and the steel plate strength has the least influence on the deflection reduction coefficient, and the specimen maintains a strong rigidity. When the concrete strength is C40, the deflection reduction coefficients of IWST of 12 mm and 8 mm are significantly smaller than that of IWST of 10 mm. With the decrease of the strength of the steel plate, the gap is also decreasing. At this time, the bearing capacity of the specimen is not controlled by a single parameter. When the concrete strength increases to C50, the IWST and the steel plate strength have little effect on the deflection reduction coefficient, indicating that the concrete strength is the main factor affecting the deflection of the joint.

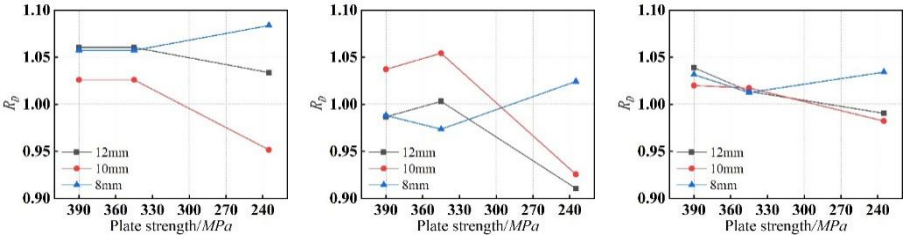

（a）The concrete strength is C30　（b）The concrete strength is C40　（c）The concrete strength is C50

Fig. 8. The influence of the IWST on R_D

In summary, the IWST has less influence on the bearing capacity index of the specimen than the two parameters of concrete strength and steel plate strength. When the strength of concrete and steel plate is larger, the influence is smaller. Combined with the above analysis, when the steel plate strength is Q345 and the concrete strength is C50, the thickness of the IWST has less influence on the bearing capacity of the specimen and is more stable.

4 Conclusion

In this paper, based on the prefabricated underground granary composite wall specimen, combined with the previous analysis of the research group, based on the finite element simulation, the bearing capacity reduction coefficient (peak load reduction coefficient and deflection reduction coefficient) is calculated and analyzed for the three parameters affecting the bearing capacity of the joint. Through the analysis, the following conclusions are obtained:

1) As the concrete strength intensifies, the peak load reduction coefficient is on the rise as a whole, and the deflection reduction coefficient has no obvious increase or decrease.

2) The steel plate strength is positively correlated with the reduction coefficient of peak load, and the reduction coefficient of deflection is larger when the steel plate strength is lower.

3) The IWST has little effect on the bearing capacity reduction coefficient.

4) The strength of concrete has the greatest influence on the bearing capacity reduction coefficient of the specimen, followed by the strength of the steel plate, and the IWST has the least influence. When the concrete strength is C50, the steel plate strength is Q345 and IWST is 10 mm, the bearing capacity reduction coefficient of the specimen is the most stable, which can provide reference for the design of the structure in the actual project.

Reference

1. Dunkel, F.V. (1995). Applying current technologies to large-scale, underground grain storage. Tunnelling and Underground Space Technology, 10(4): 477–496.
2. Chuai, J., Hou, Z.L., Wang, Z.Q. (2020). Mechanical Properties of the Vertical Joints of Prefabricated Underground Silo Steel Plate Concrete Wall. Advances in Civil Engineering, 1–18.
3. Pan, Y., Yi, D., Wu, W., Bao, Y., & Guo, R. (2020). Mechanical performance test and finite element analysis of prefabricated utility tunnel L-shaped joint. The Structural Design of Tall and Special Buildings.
4. Campos, U., Hall, D., Azimi, M., Matthews, J., Alam, S., Morgan, C., & Baghi, H. (2020). Experimental and numerical analysis of the assembly and disassembly of an interlocking joint with large diameter pipe applications. Tunnelling and Underground Space Technology, 98, 103332.
5. He, H.F., Li, Z.P. (2021). Effect Mechanism of Connection Joints in Fabricated Station Structures. Appl Sci-Basel ,11(24).
6. Liu, H., Wang, Z., Du, X., & Shen, G. Q. P. (2021). The seismic behaviour of precast concrete interior joints with different connection methods in assembled monolithic subway station. Engineering Structures, 232, 111799.
7. Gong, C., Ding, W., Soga, K., & Mosalam, K. M. (2019). Failure mechanism of joint waterproofing in precast segmental tunnel linings. Tunnelling and Underground Space Technology, 84: 334–352.
8. Feng, K., He, C., Qiu, Y., Zhang, L., Wang, W., Xie, H., Cao, S. (2018). Full-scale tests on bending behavior of segmental joints for large underwater shield tunnels. Tunnelling and Underground Space Technology, 75:100–116.
9. Jin, H., Yu, S., Zhou, S., & Xiao, J. (2018). Research on Mechanics of Longitudinal Joint in Shield Tunnel by the Nonlinear Spring Equivalent Method. KSCE Journal of Civil Engineering, 23(2): 902–913.
10. Lubliner, J., Oliver, J., Oller, S. (1989). A plastic-damage model for concrete. International Journal of Solids and Structures, 25(8): 299—329.
11. Lee, J., Fenves, G.L. (1998). Plastic-damage model for cyclic loading of concrete structures. Journal of Engineering Mechanics, 124(8): 892—900.
12. Salguero, F., Romero, S., Prat, F., Arribas, R., & Moreno, F. (2014). Universal Stress-Strain Equation for Metallic Materials. Journal of Materials in Civil Engineering, 26(8), 04014030.
13. Zhang, H., Wang, H.K., Yang, J.P., Wang, F.M. (2023). A novel vertical waterproofing joint with trapezoidal steel plate connections for steel–concrete underground silos: Bending test and numerical simulation. Tunnelling and Underground Space Technology, 137, 105150.